C. R. Mecanique 346 (2018) 877–886

Contents lists available at ScienceDirect

Comptes Rendus Mecanique

www.sciencedirect.com

Numerical study on the shear-flow behavior and transport process in rough rock fractures

Yubao Zhang [a], Na Huang [b,c,*]

[a] State Key Laboratory of Mining Disaster Prevention and Control Co-founded by Shandong Province and the Ministry of Science and Technology, Shandong University of Science and Technology, Qingdao, Shandong 266590, China
[b] School of Petroleum Engineering, China University of Petroleum (East China), Qingdao, Shandong 266580, China
[c] School of Engineering, Nagasaki University, 1-14 Bunkyo-machi, 8528521 Nagasaki, Japan

ARTICLE INFO

Article history:
Received 23 February 2018
Accepted 27 May 2018
Available online 23 June 2018

Keywords:
Rock fracture
Shear effects
Hydro-mechanical behavior
Solute transport

ABSTRACT

This paper presents a systematic research for understanding mechanical shearing effects on the fluid flow and the solute transport behavior of rough fractures through a numerical simulation approach. The aperture fields were modeled based on a real rock fracture geometry and the normal displacement obtained from the shear-flow test. The fluid flow through the rough fracture under shear was simulated using a finite element code that solves the Reynolds equation, and the transport behavior through the rough fracture under shear was simulated calculating the advection–dispersion equation. The results show that the fracture apertures increase as the shear displacement increases, with a few major flow channels detected through the fracture. The shear-induced flow channels increase both flow connectivity and transport connectivity, which accelerate the movement of solutes in a particular direction and lead to early breakthrough of the contaminants. Adsorption, acting as a retardation term, has a decisive influence on the transport process. These results can give a basic knowledge of the hydromechanical and solute transport progress through fracture, and will be helpful to safety assessment for high-level radioactive waste disposal facilities.

1. Introduction

Groundwater circulation and contaminant migration in rock fractures have attracted substantial attention for the development and utilization of deep underground spaces such as landfill reservoirs, geothermal energy plants, and radioactive waste repositories [1–3]. The excavations of these engineering works modify the stress field and induce deformations of the pre-existing joints in the rock mass, which alter the fluid flow and solute transport. While an increase in normal loading tends to close the fracture, shear displacement may open fractures due to dilation and result in significant channeling effect, which would increase its permeability and accelerate the migration of solutes in a particular direction [4–7]. This has a significant impact on radioactive waste repositories in fractured rocks, since their performance is mainly based on the knowledge of waste transport paths and travel times.

Many efforts have been made to analyze the characteristic of fluid flow and solute transport processes in rock fracture [8–12]. The shear-flow test in fractured rocks is of great importance to understand and quantify the behavior of fluid flow

* Corresponding author.
E-mail address: lixuehn@126.com (N. Huang).

https://doi.org/10.1016/j.crme.2018.05.006
1631-0721/

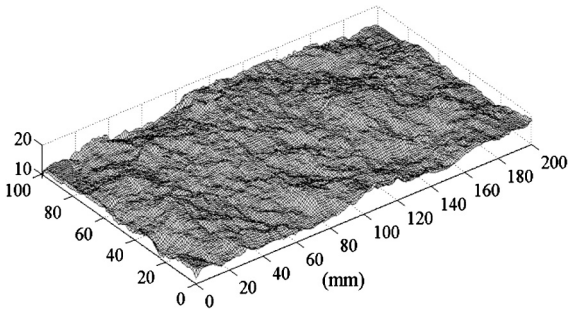

Fig. 1. Three-dimensional surface topographies of the sample.

and solute transport. Saito et al. [13] conducted a series of permeability shear tests on the specimens made artificially, and concluded that, during the shear process, the fracture tends to be more heterogeneous and permeable. Similar conclusions were obtained by Esaki et al. [14], who showed that transmissivity increases rapidly during shearing, by about 1.2 to 1.6 orders of magnitude within the first 5 mm of shear displacement, and Chen et al. [15], who highlighted the need for considering surface roughness and tortuosity when estimating the hydraulic characteristics during shearing. These studies investigated the permeability anisotropy and quantified the evolutions of hydraulic aperture based on hydromechanical shear experiments. Unfortunately, during the progress of the experiment, direct measurements and visualizations of transmissivity and flow paths inside the tested fracture specimens are generally not possible, especially during shearing. Therefore, many researchers [16–20] resorted to numerical simulations to overcome some of these drawbacks. In their studies, however, to avoid solving ill-formed matrix equations in simulations, very small aperture values were assigned to the contact spots. Thus, there still exist some artificial flows, despite small in magnitude, inside the contact areas. To address this question, Koyama et al. [21] proposed a special algorithm to treat the contact areas as zero-aperture elements, which could produce more accurate flow field and make possible continued simulations of solute transport. These findings are not only important for a more physical understanding of the coupled shear-flow behavior, but also of great help to simulate the solute transport process in fractured rocks in a more realistic fashion.

The process of mass transport through rock fractures includes many different mechanisms, such as advection, hydrodynamic dispersion, sorption reaction, and matrix diffusion [22]. Since the 1960s, many numerical simulations, analytical studies, or laboratory experiments have been performed to study contaminant transport behaviors in rock fractures [23–25]. Numerical simulation methods for solute transport in rough fractures for various initial and boundary conditions have been widely used to consider the transport mechanisms mentioned above. Among them, transport simulation with stochastic aperture for a single fracture was conducted by Wendland and Himmelsbach [26], and the results were compared with those of a laboratory experiment. Additionally, many solutions in analytical forms for different boundary conditions were also proposed [27,28]. Although these studies have considered many processes, mechanisms, and factors, they neglected the effect of shearing on the transport process in rough fractures.

Overall, the shear flow behavior and solute transport in rough factures have been widely investigated independently. However, the effects of shear on solute transport have not been extensively studied. In the present study, the effects of mechanical shearing on fluid flow and solute transport were studied by numerical modeling. The study is divided into three steps: the first one is a basic study of fracture aperture distributions and their evolution during shearing, combined with measured surface topographical data, and shear dilations obtained from a laboratory test. In the second step, based on the aperture evolution pattern drawn from the first step, the study was extended to investigate the effect of shear-induced channels on transmissivity and flow anisotropy, considering the natural roughness of the fracture surface, which was incorporated into the simulation model by assignation of spatially variable apertures to fracture elements. The third step added solute transport processes to the fluid flow field, including both non-sorbing and sorbing species, so that the impact of shear stress on transport properties can be evaluated. Artificial rough rock fractures were used to model the flow and transport with a numerically simulated shearing process under constant normal stress. The hydromechanical process and mass transport behavior were discussed based on the simulation results.

2. Estimation of aperture and transmissivity during shearing

The rough fracture specimen and experimental results by Xiong et al. [29] were used in this study to simulate more realistically the shearing process. The artificial fracture specimen J3 used in the experiment is 200 mm in length, 100 mm in width, and 100 mm in height, and is composed of upper and lower halves. The upper and lower surfaces of a fracture were supposed to be fully mated, thus the initial contact ratio was very close to 1.0. The surface of the specimen was measured by using a three-dimensional laser scanning profilometer system to build the geometrical models as shown in Fig. 1. The fracture has a very rough surface with plenty of small asperities, of which JRC ranges 17–18 [29]. Once the specimens were set in the shear box, the lower half was fixed, and the upper half can move in vertical and horizontal directions without rotating during shearing. The relation between the normal displacement and the shear displacement

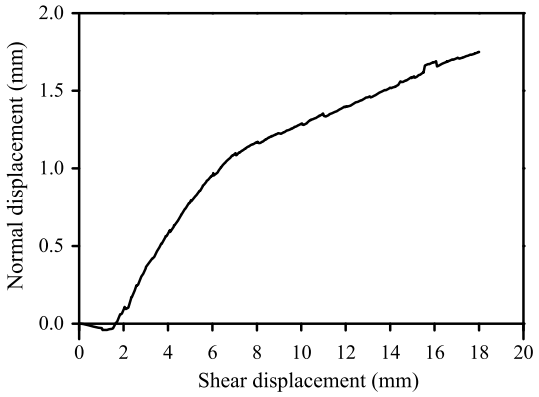

Fig. 2. Normal displacement versus shear displacement.

obtained from the test is shown in Fig. 2. More details about the experiment are available in the study of Xiong et al. [29], and we refer the interested reader to it for specific information.

During the shear process, the mean mechanical aperture b_{m} can be assessed according to the following equation [14]:

$$b_{\mathrm{m}} = b_0 - \Delta b_{\mathrm{n}} + \Delta b_{\mathrm{s}} \tag{1}$$

where b_0 is the initial aperture, Δb_{n} is the change of aperture due to normal loading, and Δb_{s} is the change of aperture induced by shear. The initial mechanical aperture can be determined by a cyclic loading–unloading test, and also can be obtained directly by using the measured hydraulic aperture before shearing [30,31]. Under constant normal load (CNL) boundary conditions, Δb_{n} could be taken as a constant. Δb_{s} is the measured normal displacement during shear.

Shearing is simulated by fixing the lower surface and moving the upper surface by a horizontal shear displacement d_{s}, then uplifting by the dilation increment based on the normal displacement d_{n} at the corresponding shear interval. Consequently, the local aperture b_{ij} at any point (i, j) with an interval of 0.2 mm can be determined. The locations where apertures are equal to or less than zero represent contact areas, and crushing of the weakest fracture asperities due to shearing is not considered.

When translational shear and normal displacement are enforced numerically, as mentioned above, the whole previous contact pattern is broken and some new contact areas and voids are generated; therefore, at each shear interval the contact conditions and apertures have to be re-evaluated for all elements [19–21]. After the aperture field at each shear step is known, the natural roughness of the fracture surface can be added to the finite model by assignation of these spatially variable apertures to fracture elements. Assuming that the cubic law is valid locally within the elements, the transmissivity, T, of each FEM element can be expressed as

$$T = \frac{\rho g b^3}{12\mu} \tag{2}$$

where ρ is the fluid density, g is the gravitational acceleration, μ is the dynamic viscosity, and b is the mean local fracture aperture, calculated using Eq. (1). In this study, the characteristics of water used at 10 °C were $\rho = 999.7$ kg/m^3, and $\mu = 1.307 \times 10^3$ Pa·s, with $g = 9.807$ m/s^2. Therefore, the transmissivity evolution during shearing can be obtained by using a determined contact pattern and an aperture field at each shear interval.

3. Numerical simulations of fluid flow and solute transport

3.1. Numerical simulations of fluid flow

When the flow velocity is low and the fracture surface geometry does not vary too abruptly, an approximate solution, which consists in dividing the void space between the two fracture surfaces into a lot of small simplified parallel plates, can be used to describe the flow in fractures instead of the full Navier–Stokes equation [32,33]

$$\nabla \cdot (T \nabla h) + Q = 0 \tag{3}$$

where h is the hydraulic head, and Q is the source term.

The discretized FEM formulation of Eq. (3) when applied to the Galerkin scheme can be written as:

$$\sum_{m=1}^{N} [K^{(m)}]\{h^m\} = \sum_{m=1}^{N} \{F^{(m)}\} \tag{4}$$

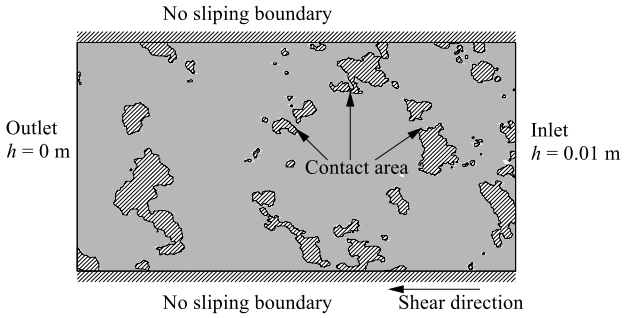

Fig. 3. Boundary conditions of fluid flow through the rock fracture.

with

$$\left[K^{(m)}\right] = \int_{S^{(m)}} \left[B^{(m)}\right]^{\mathrm{T}} \left[D^{(m)}\right] \left[B^{(m)}\right] \mathrm{d}S \tag{5}$$

$$\left\{F^{(m)}\right\} = \int_{S^{(m)}} \left[N^{(m)}\right]^{\mathrm{T}} Q^{(m)} \mathrm{d}S - \int_{L^{(m)}} \left[N^{(m)}\right]^{\mathrm{T}} \left(T \frac{\partial h}{\partial x} n_x + T \frac{\partial h}{\partial y} n_y\right) \mathrm{d}L \tag{6}$$

where N is the total number of elements, m is the element number, n_x represents the unit normal vector to the boundary in the x direction, n_y represents the unit normal vector to the boundary in the y direction, $[K^{(m)}]$ is the local transmissivity matrix, $\{F^{(m)}\}$ is flux vector, and $S^{(m)}$, $[N^{(m)}]$, $\{h^{(m)}\}$ and $L^{(m)}$ are surface area, shape function matrix, and the boundary in which the flow rate is known, respectively. The matrices $[D^{(m)}]$ and $[B^{(m)}]$ are defined as

$$\left[D^{(m)}\right] = \begin{bmatrix} T & 0 \\ 0 & T \end{bmatrix} = \begin{bmatrix} \frac{\rho_{\mathrm{f}} g {b^{(m)}}^3}{12\mu} & 0 \\ 0 & \frac{\rho_{\mathrm{f}} g {b^{(m)}}^3}{12\mu} \end{bmatrix} \tag{7}$$

$$\begin{Bmatrix} \frac{\partial h}{\partial x} \\ \frac{\partial h}{\partial x} \end{Bmatrix} = \begin{Bmatrix} \frac{\partial [N^{(m)}]^{\mathrm{T}}}{\partial x} \\ \frac{\partial [N^{(m)}]^{\mathrm{T}}}{\partial y} \end{Bmatrix} \left\{h^{(m)}\right\} = \left[B^{(m)}\right] \left\{h^{(m)}\right\} \tag{8}$$

The commercial FEM software COMSOL Multiphysics was used to solve Eq. (3). Each boundary of the fracture model was divided with an edge length of 0.1 mm, and the whole fields were divided into 2000 × 1000 small square grids. As shown in Fig. 3, the simulated flow boundary condition is to fix the initial hydraulic heads of 0.01 m and 0 m along the right- and left-hand-side boundaries, respectively. No-flux boundary conditions are imposed on the other two boundaries. A special algorithm is imposed on the contact areas to numerically eliminate them from the calculation domain, and their boundaries are zero normal flux conditions.

3.2. Numerical simulations of solute transport

The calculated flow fields are used to predict the migration of solute through rough fractures at each shear step. This can be accomplished by direct resolution of the advection–dispersion equation (ADE):

$$\frac{\partial c}{\partial t} = -\boldsymbol{V} \nabla c + \nabla \cdot (\boldsymbol{D} \nabla c) \tag{9}$$

where $\boldsymbol{V}$ is the actual fluid velocity, the solute concentration c is a dimensionless quantity normalized to the inlet concentration:

$$c(x, y) = \frac{C(x, y)}{C_{\mathrm{inlet}}} \tag{10}$$

where C_{inlet} is the inlet concentration, $C\ (x, y)$ is the solute concentration at point (x, y). $\boldsymbol{D}$ is the hydrodynamic dispersion coefficient, and it can describe the spreading of a solute pulse that is induced by local variations of flow velocity and molecular diffusion [34]. In the parallel plate model, dispersion coefficient D_{ij} is defined as

$$D_{xx} = \frac{1}{\sqrt{v_x^2 + v_y^2}} \left(\alpha_{\mathrm{L}} v_x^2 + \alpha_{\mathrm{T}} v_y^2\right) + D_{\mathrm{m}} \tag{11}$$

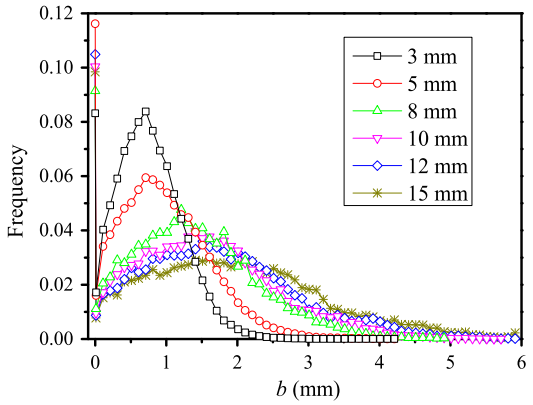

Fig. 4. Frequency curves of aperture distributions for different values of shear displacement.

$$D_{xy} = D_{yx} = \frac{1}{\sqrt{v_x^2 + v_y^2}}(\alpha_{\mathrm{L}} - \alpha_T)v_x v_y + D_{\mathrm{m}} \tag{12}$$

$$D_{yy} = \frac{1}{\sqrt{v_x^2 + v_y^2}}\left(\alpha_{\mathrm{T}} v_x^2 + \alpha_{\mathrm{L}} v_y^2\right) + D_{\mathrm{m}} \tag{13}$$

where v_x and v_y are fluid velocities in the x- and y-directions, α_{L} and α_{T} are the longitudinal dispersivity and transverse dispersivity, respectively, and D_{m} is the molecular diffusion coefficient. The ADE is solved locally for a given aperture distribution and flow field determined from the resolution of the Reynolds equation of every small simplified parallel-plate. Initially, the fluid in the fracture at each shear step is solute-free. At time $t = 0$, the dimensionless concentration at inlet is set to 1.0. Then the time-dependent solution to Eq. (9) can provide a description of solute distribution in fracture fluid.

The average solute concentration $\bar{c}$ at the outlet can be computed according to

$$\bar{c} = \frac{\int_0^L c(x, y)h(x, y)\mathrm{d}y}{\int_0^L h(x, y)\mathrm{d}y} \tag{14}$$

where L represents the fracture sample width. The average solute concentration at the outlet can be plotted in terms of a concentration breakthrough curve. The breakthrough curve will be analyzed by fitting it to the analytic error function solution to a one-dimensional advection dispersion equation, which reads [35]:

$$c(x, t) = \frac{1}{2}\left[\mathrm{erfc}\left(\frac{x - Vt}{2\sqrt{D_{\mathrm{L}}t}}\right) + \exp\left(\frac{Vx}{D_{\mathrm{L}}}\right)\mathrm{erfc}\left(\frac{x + Vt}{2\sqrt{D_{\mathrm{L}}t}}\right)\right] \tag{15}$$

where V is the effective velocity, and D_{L} is the longitudinal dispersion coefficient. Eq. (15) applies strictly for a smooth fracture of constant aperture with uniform fluid velocity and zero dispersion. In the application of this equation to rough fractures, both the effective velocity V and the dispersion coefficient D_{L} are taken as adjustable parameters to fit the breakthrough curves [36]. The fitting results can be used to estimate the Péclet number, which can give a measure of relative degree of channeling effect in fracture fluid flow [37,38]:

$$Pe = \frac{VL}{D_{\mathrm{L}}} \tag{16}$$

4. Results

4.1. Fluid flow patterns during shearing

The frequency curves of aperture distributions under displacement are shown in Fig. 4. The apertures with $b = 0$ indicate the contact areas between the upper and lower fracture surfaces. The frequency curves change from sharp to flat as the shear displacement increases, with a decreased peak value of the frequency curves. This indicates that the aperture field becomes more anisotropic and heterogeneous as the shear displacement increases. Fig. 5 shows the evolutions of aperture distributions with shear displacement, superimposed with an arrow indicating the overall flow direction. In this figure, the gray intensity of the background indicates the magnitude of local aperture, and the white isolated regions represent the contact areas. The simulation results show that, at a small shear displacement of 3 mm, a few flow channels appear in the void areas, though not very apparently, following a tortuous path bypassing plenty of small contact obstacles. As the shear

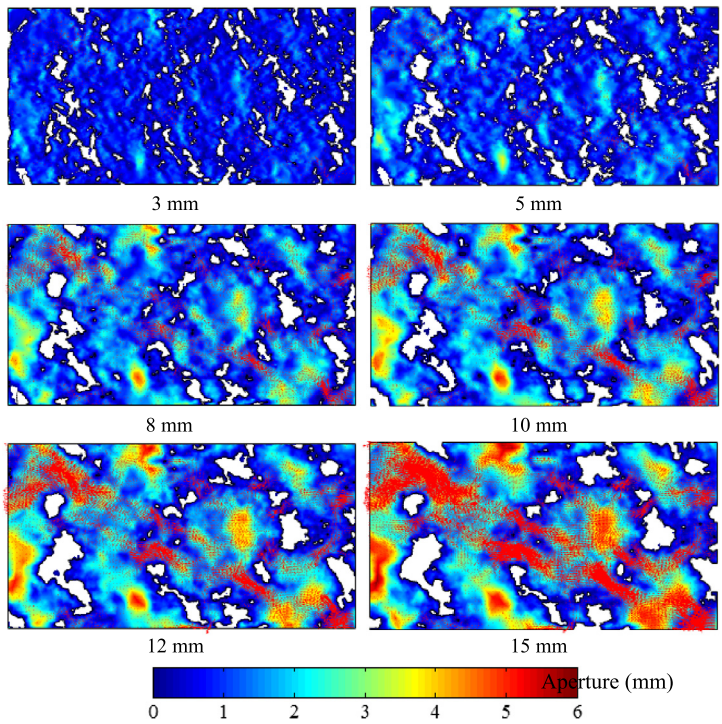

Fig. 5. Evolution of aperture and flow velocity fields with shear displacement.

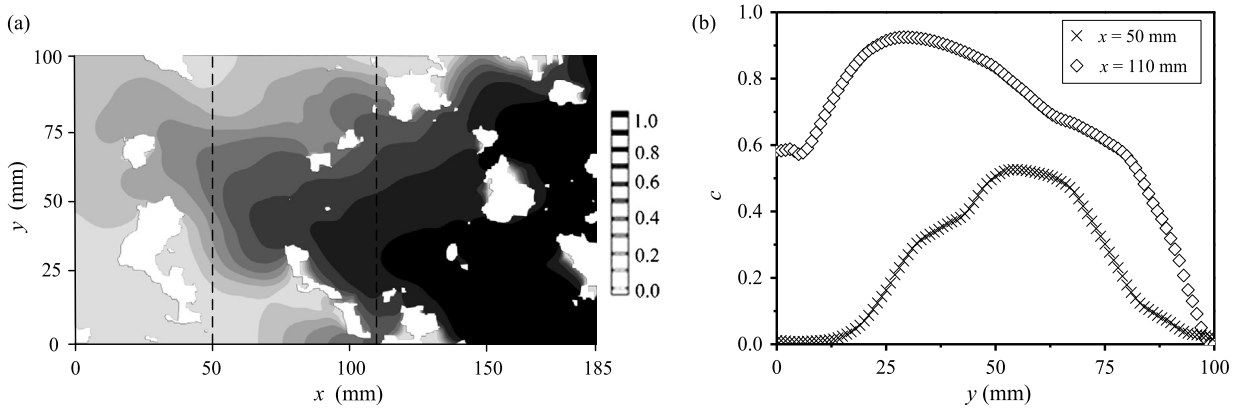

Fig. 6. Concentration contour during solute transport, (a) Concentration isoline during solute transport, (b) concentration distribution at $x = 50$ mm and $x = 110$ mm.

moves on, more continuous and obviously flow paths start to form and continue to grow with an increase in aperture and a decrease in contact areas. Most of the flow concentrates into a few major channels after a shear displacement of 5 mm, while the contact areas focus at much fewer locations of larger areas, which remain almost constant. In general, the overall flow pattern is very tortuous. This phenomenon is the well-known 'channeling effect' [39]. At present, due to the difficulty of direct measurement and visualization, the process of complex evolution of flow localization during shear can only be illustrated realistically by a numerical simulation method.

4.2. Solute transport during shearing

An example of concentration contour at the shear interval of 15 mm is shown in Fig. 6a. It is noted that the solute front exhibits a preference for some flow channels that have been contaminated by the solute with high concentrations. On the contrary, the regions of law transmissivity tend to be contaminated much more slowly. These regions will be eventually contaminated, but only after a few times. Fig. 6b shows a concentration distribution at positions $x = 50$ mm and $x = 110$ mm in Fig. 6a. This further demonstrates the characteristics of non-uniformity and anisotropy for the transport of solute in rough fracture.

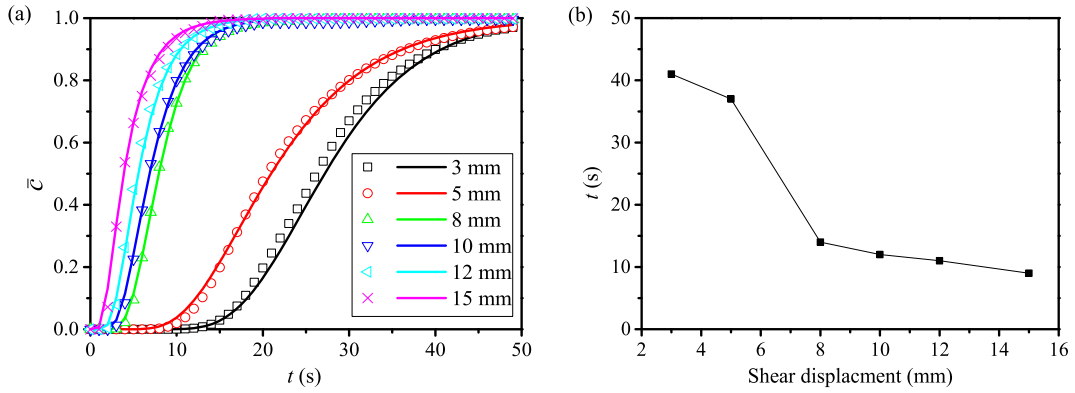

Fig. 7. (a) Comparison of concentration breakthrough curves at outlet during shearing. The scatter plots are results of numerical simulation and the solid curves are analytical solutions. (b) Time needed for the concentration at outlet to reach 90% for different values of shear displacement.

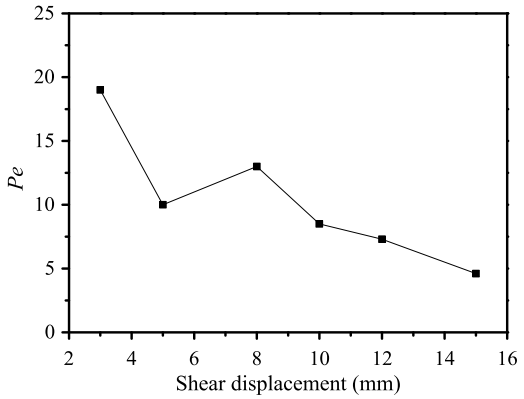

Fig. 8. Evolution of the Péclet number during shearing.

Fig. 7a displays the concentration breakthrough data and their changes during shear. The scatter plots represent the two-dimensional numerical solutions, and the solid curve displays the fitting results against the 1-D analytical solution (Eq. (15)). The shape of each breakthrough curve indicates that there is the phenomenon of both early rise and lag behind of solute concentration, which is due to the fact that some solute moves through the fast fluid flow channels directly, while others have to bypass more contact areas and transport in the low-aperture regions with very small velocity. It can also be observed that the breakthrough curve shifts leftward gradually with the increase of shear displacement, so that it takes less time for the rock fractures to be contaminated. This tendency can also be observed by comparing the time needed for the concentration of outlet to reach to 90% at different values of the shear displacement (Fig. 7b). The decrease of the travel time is much more apparent during the early stage of shearing, especially between the shear displacements of 5 and 8 mm. One interpretation is that shearing makes the fracture more hydraulically conductive with higher velocity, and on the other side, the higher flow velocity is, the less time it takes for the solute to travel through fracture. Correspondingly, the significant increase of flow velocity from the shear displacement of 5 to 8 can be seen in Fig. 5.

The comparison of the Péclet numbers for rough fractures at different shear interval is shown in Fig. 8. The effective dispersivities obtained from the curve-fitting results are used for back-calculations of the Péclet number. In this analysis, the calculated Péclet numbers are between 4 and 20, and agree well with those determined in laboratory measurements and numerical tracer tests in rough fractures (Table 1). In general, the Péclet number decreases with the increasing shear displacement, though some exception is observed, and the decrease in the Péclet number corresponds to an increasing dispersivity. This trend reflects the fact that dispersion becomes more significant and tends to dominate solute migration as shearing progresses. One interpretation for this may be the fact that the increasing shear displacement concentrates the contact areas and induces fast flow and travel channels, which produces higher dispersivity for overall rough fracture.

4.3. Effect of adsorption during shearing

Mass transport through rock fractures is a complex natural phenomenon including many different mechanisms, among which the adsorption of chemical species onto fracture surfaces is also one considerable issue. Adsorption, acting as an important retarding mechanism, can substantially reduce the concentration of solute in the fracture fluid. The simplest adsorption model assumes instantaneous equilibrium reaction, in which the concentration of species adsorbed onto the

Table 1
Comparison of the Péclet numbers in experimental and numerical tests.

Research	Sample length (cm)	Rock type	*Pe* range
Neretnieks et al. [40]	30	Granite	9–27
Moreno et al. [41]	27	Granite	9–80
Moreno et al. [23]	Dimensionless	Stochastically generated fracture	2–40
Thompson [36]	100	Stochastically generated fracture	3–50
This study	20	Artificial fracture	4–20

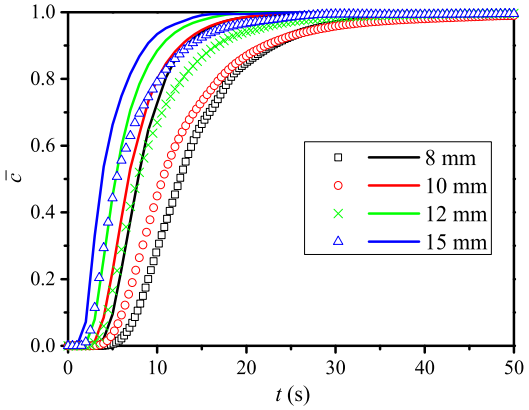

Fig. 9. Comparison of breakthrough curves for sorbing and non-sorbing species for different values of shear displacement. Scatter plots are the results for sorbing species, and the solid curves are the results for non-sorbing species.

fracture surface c_s is proportional to the fluid concentration c. The proportionality factor is termed as the surface adsorption coefficient K_s and is defined as [36]:

$$c_s = K_s c \tag{17}$$

The adsorption can be incorporated into solute transport process by defining a retardation factor R_f

$$R_f = 1 + \frac{2K_s}{h(x, y)} \tag{18}$$

Therefore, the transport equation considering adsorption mechanics is

$$R_f \frac{\partial c}{\partial t} = -\mathbf{V}\nabla c + \nabla \cdot (\mathbf{D}\nabla c) \tag{19}$$

To investigate the adsorption processes in rough rock fractures during shearing, Eq. (19) is solved and the obtained breakthrough curves are analyzed in the same manner as for non-sorbing species. The numerical breakthrough curves for sorbing species are compared to those for non-sorbing species (Fig. 9). The solid curves represent the simulation results for the non-sorbing solute and the scatter plots represent the simulation results for the sorbing solute. The comparison results show that adsorption acts to retard solute migration, resulting in an overall slag of the breakthrough curves. The effect of adsorption in slowing down transport is more significant at smaller shear displacements. This is because, as shear displacement increases, even though the contact areas tend to decrease and a greater percentage of surface area is available for the sorption reaction, the surface adsorption coefficient K_s decreases with an increasing of the effective hydraulic aperture.

As often observed in the natural system, due to the roughness of the fracture surface, the hydraulic properties of fractured rocks are usually scale-dependent. The distribution of aperture during shearing varies with the sample size, which will result in different flow patterns and solute transport paths. The analysis of one fracture specimen with dimensions 200 × 100 × 100 mm in this study is limited, and more models with varying sizes are needed for a general representation of fracture characteristic. Another limitation of the analyses in this study is that the influences of shearing rate on the variation of permeability and transport fields are not considered. The reason for excluding this factor is the limitation of experimental condition. However, this is an important issue, since the shearing rate will affect the hydraulic response significantly, and this should be investigated in future works.

5. Conclusions

Fluid flow and solute transport in rough rock fracture subjected to shear was studied numerically. The fracture aperture distributions and its evolution during shearing were evaluated from the initial aperture, based on the measured surface

topographical data, and shear dilations obtained from the laboratory test. The natural roughness of the fracture surface was incorporated into the model by assignation of spatially variable apertures to fracture elements. Then the flow in rough fracture was simulated using the Reynolds equation, and the movement of solute including both non-sorbing and sorbing species in rough fracture undergoing shear was studied by solving the advection–dispersion equation. The macroscopic transport properties of fractures are derived in comparison of the numerical simulations with predictions of one-dimensional advection dispersion model. This makes it possible to determine effective dispersivities and solute velocities for rough surfaces. Correspondingly, the change in flow paths and Péclet number during shear were also examined.

The results suggest that shear displacements lead to an increase in the magnitude of flow rates and solute velocity. The increase is mainly due to the change of void space geometry and contact area distribution, thus the accurate description of the evolution of those geometry characteristics during shear is important for the prediction of the flow and transport behavior for rough fractures. Shear-induced channels lead to the characteristics of non-uniformity and anisotropy for mass transport in rough fracture. As shear displacement increases, large apertures are generated with a few major flow channels existing in the fracture, which accelerates the movement of solutes in a particular direction, and leads to early breakthrough of the contaminants. More significant and obvious flow paths continue to grow with the shear moving on. This leads to a large variance in travel time. Correspondingly, as indicated by the decreasing Péclet number, dispersion gradually plays an important role in the overall transport migration during the shear progress. In the future, the investigations will be extended to study the flow and transport behavior through the two-dimensional and three-dimensional fracture networks, and to study how the mechanical load impacts flow connectivity and transport connectivity.

Acknowledgements

This study has been partially funded by the National Natural Science Foundation of China (No. 51604165) and the China Scholarship Council (No. 201708370105). These supports are gratefully acknowledged.

References

[1] J.S. Hanor, Effective hydraulic conductivity of fractured clay beds at a hazardous waste landfill, Louisiana Gulf Coast, Water Resour. Res. 29 (11) (1993) 3691–3698.
[2] C.F. Tsang, F. Bernier, C. Davies, Geohydromechanical processes in the Excavation Damaged Zone in crystalline rock, rock salt, and indurated and plastic clays—in the context of radioactive waste disposal, Int. J. Rock Mech. Min. Sci. 42 (1) (2005) 109–125.
[3] J. Bundschuh, Introduction to the Numerical Modeling of Groundwater and Geothermal Systems: Fundamentals of Mass, Energy and Solute Transport in Poroelastic Rocks, CRC Press, Boca Raton, FL, USA, 2010.
[4] L. Moreno, C.F. Tsang, Y. Tsang, et al., Some anomalous features of flow and solute transport arising from fracture aperture variability, Water Resour. Res. 26 (10) (1990) 2377–2391.
[5] R. Liu, B. Li, Y. Jiang, et al., A numerical approach for assessing effects of shear on equivalent permeability and nonlinear flow characteristics of 2-D fracture networks, Adv. Water Resour. 111 (2018) 289–300.
[6] N. Huang, R. Liu, Y. Jiang, et al., Effects of fracture surface roughness and shear displacement on geometrical and hydraulic properties of three-dimensional crossed rock fracture models, Adv. Water Resour. 113 (2018) 30–41.
[7] Q. Zhang, C.H. Zhang, B.S. Jiang, N. Li, Y.C. Wang, Elastoplastic coupling solution of circular openings in strain-softening rock mass considering pressure-dependent effect, Int. J. Geomech. 18 (1) (2018) 04017132.
[8] J. Cai, W. Wei, X. Hu, et al., Fractal characterization of dynamic fracture network extension in porous media, Fractals 25 (02) (2017) 1750023.
[9] W. Wei, Y. Xia, Geometrical, fractal and hydraulic properties of fractured reservoirs: a mini-review, Adv. Geo-energ. Res. 1 (1) (2017) 31–38.
[10] B. Li, R. Liu, Y. Jiang, Influences of hydraulic gradient, surface roughness, intersecting angle, and scale effect on nonlinear flow behavior at single fracture intersections, J. Hydrol. 538 (2016) 440–453.
[11] R. Liu, B. Li, Y. Jiang, Critical hydraulic gradient for nonlinear flow through rock fracture networks: the roles of aperture, surface roughness, and number of intersections, Adv. Water Resour. 88 (2016) 53–65.
[12] R. Liu, B. Li, Y. Jiang, A fractal model based on a new governing equation of fluid flow in fractures for characterizing hydraulic properties of rock fracture networks, Comput. Geotech. 75 (2016) 57–68.
[13] R. Saito, Y. Ohnishi, S. Nishiyama, T. Yano, S. Uehara, Hydraulic characteristics of single rough fracture under shear deformation, in: ISRM International Symposium, EUROCK 2005, 2005.
[14] T. Esaki, S. Du, Y. Mitani, K. Ikusada, L. Jing, Development of a shear-flow test apparatus and determination of coupled properties for a single rock joint, Int. J. Rock Mech. Min. Sci. 36 (5) (1999) 641–650.
[15] Z. Chen, S.P. Narayan, Z. Yang, S.S. Rahman, An experimental investigation of hydraulic behaviour of fractures and joints in granitic rock, Int. J. Rock Mech. Min. Sci. 37 (7) (2000) 1061–1071.
[16] I.W. Yeo, F.M.H. De, R.W. Zimmerman, Effect of shear displacement on the aperture and permeability of a rock fracture, Int. J. Rock Mech. Min. Sci. 35 (8) (1998) 1051–1070.
[17] K. Matsuki, Y. Chida, K. Sakaguchi, P.W.J. Gloverb, Size effect on aperture and permeability of a fracture as estimated in large synthetic fractures, Int. J. Rock Mech. Min. Sci. 43 (5) (2006) 726–755.
[18] R. Liu, Y. Jiang, B. Li, X. Wang, A fractal model for characterizing fluid flow in fractured rock masses based on randomly distributed rock fracture networks, Comput. Geotech. 65 (2015) 45–55.
[19] N. Huang, R. Liu, Y. Jiang, Numerical study of the geometrical and hydraulic characteristics of 3D self-affine rough fractures during shear, J. Nat. Gas Sci. Eng. 45 (2017) 127–142.
[20] N. Huang, Y. Jiang, R. Liu, et al., A predictive model of permeability for fractal-based rough rock fractures during shear, Fractals 25 (05) (2017) 1750051.
[21] T. Koyama, B. Li, Y. Jiang, L. Jing, Numerical modelling of fluid flow tests in a rock fracture with a special algorithm for contact areas, Comput. Geotech. 36 (1) (2009) 291–303.
[22] J. Bodin, F. Delay, G. de Marsily, Solute transport in a single fracture with negligible matrix permeability: 1. Fundamental mechanisms, Hydrogeol. J. 11 (4) (2003) 418–433.
[23] L. Moreno, Y.W. Tsang, C.F. Tsang, F.V. Hale, I. Neretnieks, Flow and tracer transport in a single fracture: a stochastic model and its relation to some field observations, Water Resour. Res. 24 (12) (1988) 2033–2048.

[24] A.A. Keller, P.V. Roberts, M.J. Blunt, Effect of fracture aperture variations on the dispersion of contaminants, Water Resour. Res. 35 (1) (1999) 55–63.
[25] R.L. Detwiler, H. Rajaram, R.J. Glass, Solute transport in variable-aperture fractures: an investigation of the relative importance of Taylor dispersion and macrodispersion, Water Resour. Res. 36 (7) (2000) 1611–1625.
[26] E. Wendland, T. Himmelsbach, Transport simulation with stochastic aperture for a single fracture–comparison with a laboratory experiment, Adv. Water Resour. 25 (1) (2002) 19–32.
[27] I. Neretnieks, Diffusion in the rock matrix: an important factor in radionuclide retardation, J. Geophys. Res., Solid Earth 85 (B8) (1980) 4379–4397.
[28] D.C.F. Shih, Contaminant transport in one-dimensional single fractured media: semi-analytical solution for three-member decay chain with pulse and Heaviside input sources, Hydrol. Process. 21 (16) (2007) 2135–2143.
[29] X. Xiong, B. Li, Y. Jiang, T. Koyama, C. Zhang, Experimental and numerical study of the geometrical and hydraulic characteristics of a single rock fracture during shear, Int. J. Rock Mech. Min. Sci. 48 (8) (2011) 1292–1302.
[30] A. Makurat, N. Barton, N.S. Rad, S. Bandis, Joint conductivity variation due to normal and shear deformation, in: Proceedings of the International Symposium on Rock Joints, Loen, Norway, Balkema, Rotterdam, 1990, pp. 535–540.
[31] T. Koyama, B. Li, Y. Jiang, L. Jing, Numerical simulations for the effects of normal loading on particle transport in rock fractures during shear, Int. J. Rock Mech. Min. Sci. 45 (8) (2008) 1403–1419.
[32] P.A. Witherspoon, J.S.Y. Wang, K. Iwai, et al., Validity of cubic law for fluid flow in a deformable rock fracture, Water Resour. Res. 16 (6) (1980) 1016–1024.
[33] N. Huang, Y. Jiang, B. Li, et al., A numerical method for simulating fluid flow through 3-D fracture networks, J. Nat. Gas Sci. Eng. 33 (2016) 1271–1281.
[34] Z. Zhao, L. Jing, I. Neretnieks, Evaluation of hydrodynamic dispersion parameters in fractured rocks, J. Rock Mech. Geotech. Eng. 2 (3) (2010) 243–254.
[35] J.C. Parker, M.T. Genuchten, Flux-averaged and volume-averaged concentrations in continuum approaches to solute transport, Water Resour. Res. 20 (7) (1984) 866–872.
[36] M.E. Thompson, Numerical simulation of solute transport in rough fractures, J. Geophys. Res., Solid Earth 96 (B3) (1991) 4157–4166.
[37] Y.W. Tsang, C.F. Tsang, I. Neretnieks, L. Moreno, Flow and tracer transport in fractured media: a variable aperture channel model and its properties, Water Resour. Res. 24 (12) (1988) 2049–2060.
[38] V. Vilarrasa, T. Koyama, I. Neretnieks, L. Jing, Shear-induced flow channels in a single rock fracture and their effect on solute transport, Transp. Porous Media 87 (2) (2011) 503–523.
[39] Y.W. Tsang, C.F. Tsang, Channel model of flow through fractured media, Water Resour. Res. 23 (3) (1987) 467–479.
[40] I. Neretnieks, T. Eriksen, P. Tähtinen, Tracer movement in a single fracture in granitic rock: some experimental results and their interpretation, Water Resour. Res. 18 (4) (1982) 849–858.
[41] L. Moreno, I. Neretnieks, T. Eriksen, Analysis of laboratory tracer runs in natural fissures, Water Resour. Res. 21 (7) (1985) 951–958.